

# Lead-Free Inorganic Nanoparticles of Perovskite Embedded within Waterproof Nanofiber Films for White Color Emission

Yongju Lee,<sup>†</sup> Ji-Hyun Cha,<sup>†</sup> Heejin Kim,<sup>†</sup> Ja Yeon Lee, Min Wook Lee,\* Ho Seong Jang,\* and Duk-Young Jung\*



Cite This: ACS Appl. Nano Mater. 2022, 5, 18409–18416



Read Online

ACCESS |

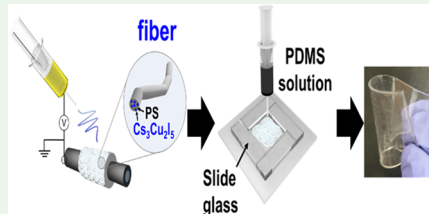
Metrics & More

Article Recommendations

Supporting Information

**ABSTRACT:** Organic polymers can enhance the environmental stability of inorganic perovskite nanocrystals (IPNCs) by encapsulation. We fabricated lead-free IPNCs embedded in waterproof and luminous polymer fibers. The encapsulated perovskite nanocrystals within polystyrene (PS) polymers,  $\text{CsCu}_2\text{I}_3@\text{PS}$  (Y-fiber), and  $\text{Cs}_3\text{Cu}_2\text{I}_5@\text{PS}$  (B-fiber) were prepared by one-step electrospinning of the solutions containing the precursors ( $\text{CsI}$  and  $\text{CuI}$ ) and PS. The embedded nanocrystals had highly uniform sizes, spatial distribution, and well-developed crystal structures. The Y- and B-fibers showed yellow and blue emission under ultraviolet (UV) light, respectively, and a white emission fiber layer was fabricated via dual-nozzle coelectrospinning using  $\text{CsCu}_2\text{I}_3$  and  $\text{Cs}_3\text{Cu}_2\text{I}_5$  precursor solutions. The as-prepared B-fibers exhibited improved water stability without changing the crystal structure and photoluminescence (PL) emission in deionized water for 20 days. To enhance environmental stability and mechanical properties, transparent poly(dimethylsiloxane) (PDMS) films containing IPNCs@PS fibers presented strong PL emission without peak shift under 100% tensile strain, indicating highly flexible and humidity-durable characteristics.

**KEYWORDS:** lead-free inorganic perovskite, hybrid fiber, emission color tuning, electrospinning, water stability



## 1. INTRODUCTION

All-inorganic  $\text{CsPbX}_3$  perovskites ( $X = \text{Cl}$ ,  $\text{Br}$ , and  $\text{I}$ ) are considered promising materials for diverse applications such as photovoltaics,<sup>1</sup> light-emitting diodes (LEDs),<sup>2</sup> and photo-detectors,<sup>3</sup> due to their intriguing optoelectronic properties.<sup>4,5</sup> Although excellent results have been reported in the research and application of lead halides, their commercialization is still limited by the toxicity of Pb and the poor stability of the materials. To address this issue, it is necessary to develop high-stability, eco-friendly broad-band emission materials. Recently, many types of lead-free perovskites have been studied to replace toxic metallic lead with other nontoxic metals, such as tin halide ( $\text{CsSnBr}_3$ ,  $\text{Cs}_2\text{SnBr}_6$ ),<sup>6,7</sup> bismuth halide ( $\text{Cs}_3\text{Bi}_2\text{Br}_9$ ),<sup>8</sup> indium halide ( $\text{Cs}_2\text{InBr}_5$ ),<sup>9</sup> and copper halide ( $\text{Cs}_3\text{Cu}_2\text{I}_5$ ,  $\text{CsCu}_2\text{I}_3$ )<sup>10,11</sup> based perovskites.

Cesium copper halide perovskites ( $\text{Cs}-\text{Cu}-\text{X}$ ) are representative light-emitting materials that are low-cost and earth-abundant, and provide eco-friendly broad-band emission. The synthesis of  $\text{Cs}-\text{Cu}-\text{X}$  compounds has been accomplished using solvent evaporation,<sup>12</sup> mechanochemical reactions,<sup>11,13</sup> QDs in surfactants,<sup>14,15</sup> melt growth,<sup>16</sup> and vapor codeposition,<sup>17,18</sup> which could be used in optoelectronic applications such as anticounteरfeiting,<sup>10,19</sup> polarization,<sup>20</sup> and white light-emitting devices (WLEDs).<sup>21,22</sup> Despite the various advantages and applications mentioned above,  $\text{Cs}_3\text{Cu}_2\text{I}_5$  perovskite has low stability in moisture, causing transformation into  $\text{CsCu}_2\text{I}_3$  and weak photoluminescence (PL) intensity.<sup>10,23</sup>

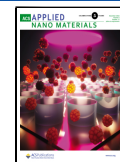
To maintain the PL emission of inorganic perovskite nanocrystals (IPNCs), appropriate protective layers are required for the encapsulation of IPNCs to prevent environmental humidity. Polymer matrixes offer thermal, moisture, and oxidation stability to IPNC materials. Several methods are suggested for improving the stability of perovskite materials through polymer coating with waterproof materials<sup>19</sup> or encapsulation within a polymer matrix.<sup>20,24</sup> Shi et al. demonstrated the reversible conversion between blue-emissive  $\text{Cs}_3\text{Cu}_2\text{I}_5$  and yellow-emissive  $\text{CsCu}_2\text{I}_3$  and a poly(methyl methacrylate) (PMMA) layer, which gives blue-emissive  $\text{Cs}_3\text{Cu}_2\text{I}_5$  long-term stability in water. Wang et al. fabricated  $\text{Cs}_3\text{Cu}_2\text{I}_5$  encapsulated in poly(vinylidene fluoride) (PVDF) nanofiber films by a one-step electrospinning technique. However, these works require complex steps or provide an irregular microparticle shape of electrospun  $\text{Cs}_3\text{Cu}_2\text{I}_5$ . The internal structure, composition control, and emission color mixing of lead-free perovskite hybrid nanofibers have been insufficiently investigated.

Here, we report a facile method for *in situ* formation of lead-free IPNCs inside polystyrene (PS) at room temperature

Received: September 26, 2022

Accepted: November 30, 2022

Published: December 14, 2022



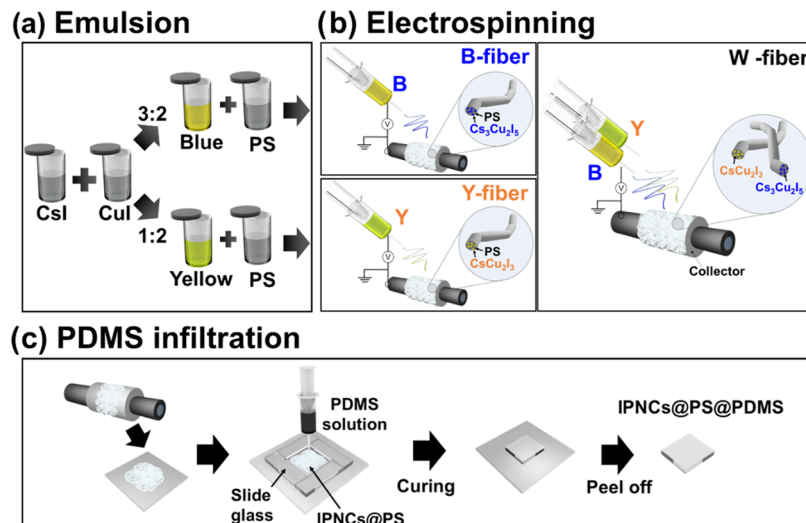


**Figure 1.** Overall procedure for the fabrication of transparent lead-free IPNCs@PS@PDMS flexible films: (a) preparation of the polymer and perovskite precursor solution, (b) electrospinning, and (c) PDMS matrix infiltration.

without organic surfactants via electrospinning of a PS and CsI/CuI precursor solution. The perovskites within PS provide uniform yellow and blue emission with a wide full width at half-maximum (FWHM). We utilized a combination of two yellow and blue emission color fibers to fabricate white light emission fiber films by coelectrospinning with a dual-nozzle system. Our encapsulation methods confirmed that coating IPNCs with PS can effectively prevent the dissolution of CsI in water and maintain blue and yellow emissions in deionized water. Also, we prepared highly stretchable and humidity-durable IPNCs@PS@poly(dimethylsiloxane) (PDMS) by applying PDMS onto IPNCs@PS fibers. Our strategies offer a low-cost and facile method for creating stable and excellent photoluminescence (PL) materials while restricting the use of surfactants and toxic chemical additives.

## 2. EXPERIMENTAL SECTION

**2.1. Materials.** All chemicals were purchased from Sigma-Aldrich and were used as received without further purification, including cesium iodide (CsI, 99.9%), copper(I) iodide (CuI, 99.999%), polystyrene (PS, M<sub>w</sub> ~ 192,000), and *N,N*-dimethylformamide (DMF, 99.5%). Resin and the curing agent for PDMS (Sylgard 184) were purchased from Dow Corning.

**2.2. Precursor of the B-Fiber.** In a 20 mL glass vial, 0.6 mmol of CsI and 0.4 mmol of CuI were dispersed in DMF, and the mixture was stirred for 30 min. After the complete dissolution of the CsI and CuI salts, a 30 wt % PS/DMF solution (1.0 g) and a CsI/CuI solution were mixed and stirred for 1 h at room temperature (Figure 1a).

**2.3. Precursor of the Y-Fiber.** For the synthesis of CsCu<sub>2</sub>I<sub>3</sub> crystals, 0.2 mmol of CsI and 0.4 mmol of CuI were dissolved in a DMF and DMSO (1:1) mixed solution, and chloroform was quickly added. A white precipitate formed and was centrifuged at 4000 rpm for 5 min.<sup>21</sup> In a 20 mL glass vial, CsCu<sub>2</sub>I<sub>3</sub> was dispersed in DMF for 30 min. After the complete dissolution of CsCu<sub>2</sub>I<sub>3</sub>, a 30 wt % PS/DMF solution (1.0 g) and CsCu<sub>2</sub>I<sub>3</sub> solution were mixed and stirred for 1 h at room temperature (Figure 1a).

**2.4. Single- and Dual-Nozzle Electrospinning of the IPNCs@PS Fiber.** A PS/perovskite mixture solution from a syringe with a stainless steel nozzle (21 G, ID/OD = 0.50/0.80 mm) was released at 0.1 mL/h using a syringe pump. A voltage supplier was connected to the nozzle, and 15 kV was applied. The IPNCs@PS fiber was collected on an Al foil-wrapped drum collector (15 cm apart at 25 °C). Dual-nozzle electrospinning was performed by two nozzles facing each other with a collector in between. Each collector–nozzle

distance and other parameters are the same as the single electrospinning condition. After electrospinning, the IPNCs@PS fibers on the substrate were heated at 120 °C for 1 h to remove residual solvent from the PS/perovskite mixed solution (Figure 1b).

**2.5. Fabrication of IPNCs@PS@PDMS Films.** A template made of a slide glass was attached to the IPNCs@PS fiber collected on an Al foil. The premixed PDMS in which resin and the curing agent were mixed in a volume ratio of 10:1 was poured into the template. After being cured at 100 °C for 10 min, the IPNCs@PS@PDMS films peeled off from the template and the Al foil. The template size was 40 × 70 mm<sup>2</sup>, and 2 mL of the premixed PDMS was used (Figure 1c).

**2.6. Characterization.** The morphologies and the sizes of the obtained products were observed by a Schottky field emission scanning electron microscope (SEM, JSM-7100F) and a field emission transmission electron microscope (FE-TEM, Tecnai G2 F20). Elemental analyses were performed using an EDS attached to a TEM. X-ray diffraction (XRD) data were collected to study the crystal structures using a Rigaku Ultima IV diffractometer with Cu K $\alpha$  radiation ( $\lambda = 1.5405 \text{ \AA}$ ). Inductively coupled plasma mass spectra (ICP-MS) were conducted using a NexION 2000 ICP-MS. PL spectra were collected on an F-7000 spectrofluorometer (Hitachi High-Tech Corp.). Ultraviolet–visible (UV-vis) spectra were recorded on a JASCO V-760 spectrometer.

## 3. RESULTS AND DISCUSSION

**3.1. In Situ Growth of Cs–Cu–I@PS Fibers and Optical Properties.** We fabricated IPNCs@PS fibers via the electrospinning process, as shown in Figure 1a,b. Briefly, precursor solutions were first prepared by blending the PS polymer and perovskite precursors in DMF solvent. Two precursor solutions with different chemical compositions were prepared for the yellow and blue emission fibers corresponding to Y- and B-fibers, respectively. Subsequently, in the electrospinning process, a liquid jet is directed toward the Al foil used as a collector, and perovskites with uniform spatial distributions were immobilized in PS fibers by rapidly evaporating solvent from fibers. Then, highly uniform PL emission of IPNCs within polymer fibers was observed (vide infra).

We controlled the two types of chemical compositions by mixing CuI and CsI to tune the emission color of the IPNCs@PS fibers. Blue color emission was indicated by forming Cs<sub>3</sub>Cu<sub>2</sub>I<sub>5</sub> from perovskite precursors with a molar ratio of CsI

and CuI of 3:2. We applied polycrystalline  $\text{CsCu}_2\text{I}_3$  for yellow emission because of the low solubility of the precursor with a CsI-to-CuI molar ratio of 1:2 in DMF. Yellow emission of the Y-fiber ( $\text{CsCu}_2\text{I}_3@\text{PS}$ ) required mild heat treatment at 90 °C, probably due to the slow recrystallization rates of  $\text{CsCu}_2\text{I}_3$ . The prepared Y-fibers showed yellow emission under 245 nm wavelength UV light without damaging the fibers, indicating the stability of encapsulated  $\text{CsCu}_2\text{I}_3$  within PS polymers against the thermal treatment (Figure S1).

The single-nozzle electrospun fibers of the two precursor solutions on the Al foil (tailored to dimensions of  $2.0 \times 2.0 \text{ cm}^2$ ) produced blue and yellow emissions under 245 nm UV light. The dual-nozzle electrospun successfully provided white light-emitting fibers (Figure 2a).  $\text{CsCu}_2\text{I}_3$  and  $\text{Cs}_3\text{Cu}_2\text{I}_5$  IPNC

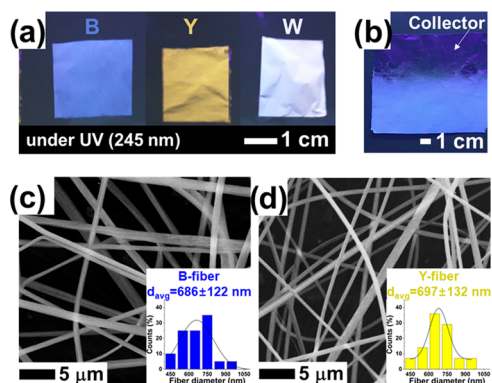


**Figure 2.** (a) Photographs of three IPNCs@PS fibers under a 245 nm UV lamp. (b) Optical images of B-fibers with a large area on the collector under a 245 nm UV lamp. SEM images of (c) B-fiber and (d) Y-fiber. The histograms in the inset show the size distribution of B- and Y-fibers.

were introduced in the fibers and demonstrated highly uniform PL emission. To estimate the contents of both IPNCs within PS fibers, quantitative analyses of the chemical compositions of the fibers were measured by an ICP-MS method, as shown in Table S1. Here, PS fibers contained 5.0 wt % IPNC on average, and the stoichiometric molar ratios of Cs/Cu were 1.40 and 0.50, consistent with theoretical data based on the formula of  $\text{Cs}_3\text{Cu}_2\text{I}_5$ , and  $\text{CsCu}_2\text{I}_3$ , respectively. In this method, the B-fibers could be electrospun up to  $5 \times 10 \text{ cm}^2$ , corresponding to the area of the collector used for electrospinning (Figure 2b). It should be noted that the electrospun fibers were applied on a large-scale area without defects. To observe the morphology and colloidal uniformity of fiber samples, SEM images were collected, as shown in Figure 2c,d. B- and Y-fibers prepared by the electrospinning method provided uniform and reproducible fiber without the formation of large beads. The average and distribution of their diameters were  $686 \pm 122$  and  $697 \pm 132 \text{ nm}$ , respectively (Figure 2c,d, inset).

To analyze the optical properties of IPNCs@PS, the luminescence spectra of the as-prepared samples under different excitation wavelengths ranging from 290 to 320 nm were further explored. As shown in Figure 3a,b, the samples exhibited broad-band emission peaks at 445 and 570 nm that are consistent with the peak positions of pristine  $\text{Cs}_3\text{Cu}_2\text{I}_5$  and  $\text{CsCu}_2\text{I}_3$ , respectively.<sup>16,25</sup> Also, the PL spectra measured at different excitation wavelengths offer the same position of a broad peak, where the B-fiber showed strong blue emission with a broad FWHM (81 nm) and the Y-fiber showed yellow

emission with a broad FWHM (99 nm) for excitation wavelengths of 290 and 320 nm, respectively.

To realize white emission, we prepared a mixture of two sources (B- and Y-fibers) using dual-nozzle electrospinning, which was performed using the same experimental conditions as for single-nozzle electrospinning, with various ratios of  $\text{Cs}_3\text{Cu}_2\text{I}_5$  and  $\text{CsCu}_2\text{I}_3$  (Figure S2). Figure 3c shows the luminescence spectrum of the as-prepared fiber with a 1:3 ratio of  $\text{Cs}_3\text{Cu}_2\text{I}_5$  to  $\text{CsCu}_2\text{I}_3$  under different excitation wavelengths ranging from 300 to 320 nm. The broad-band spectrum shows that the two phases of  $\text{Cs}_3\text{Cu}_2\text{I}_5$  and  $\text{CsCu}_2\text{I}_3$  in PS fibers cover the full range of visible light. Compared with  $\text{CsPbX}_3@\text{polymer}$  fibers,<sup>26</sup> the present B- and Y-fibers provide excellent coverage of their luminescence spectra because of the wide FWHM. The FWHM values of  $\text{Cs}_3\text{Cu}_2\text{I}_5$  and  $\text{CsCu}_2\text{I}_3$  were approximately 81 and 99 nm, respectively.

Because the PL intensities of the B- and Y-fibers depend on the excitation wavelengths, controlling excitation wavelengths is critical for producing white light emission films based on the IPNCs@PS fibers combining B- and Y-fibers. At excitation wavelengths of 300 nm, blue emission dominates yellow emission, whose CIE coordinate was ultimately (0.24, 0.22). However, at an excitation wavelength of 320 nm, yellow emission dominates blue emission, whose CIE coordinate was ultimately (0.44, 0.48). The CIE coordinate of the as-prepared emission fiber was (0.31, 0.31) under an excitation wavelength of 305 nm, which has a comparable area to the best chromaticity coordinate of white emission indicated of (0.32, 0.32) (Figure 3d).<sup>10,25,26</sup> Besides, the correlated color temperature (CCT), the key parameter for the WLED, was also measured to be 6635 K, which suggests its promising potential application in lighting fields.

### 3.2. Morphology and Structural Characterization of IPNCs.

To confirm the nanoscale structure and distribution of perovskite nanocrystals in the polymer fiber, we cut the fiber using the focused ion beam (FIB) technique. A gallium ion beam was used as a source, and cross-sectional images of the fiber were taken using a high-resolution transmission electron microscope (HR-TEM).

As shown in Figure 4a, the polymer matrix appears in bright contrast, while the perovskite nanocrystals appear dark due to the elements of perovskite, including the higher atomic number elements such as cesium (Cs), copper (Cu), and iodine (I). The perovskite nanocrystals have small sizes because of rapid crystal formation under the one-step electrospinning process, due to solvent evaporation conditions.<sup>27</sup>

Interestingly, the perovskite nanocrystals in a PS matrix have well-developed crystallinity. Figure 4b shows a clear lattice fringe (with lamellar pattern), and the  $d$  spacing is about 50 Å, which corresponds to a  $d$  value of (120) in the PXRD pattern. The magnified image in Figure 4c shows the atomic structure of the perovskite nanocrystals. The diameter of the bright circles was about 3.5 Å, which is indicated as a  $\text{Cs}^+$  atom ( $\approx 3.34 \text{ \AA}$ ). For clarity, the inset of Figure 4c depicts an image with a schematic model of C atoms presented along the [120] direction.

In Figure 4d, the fast Fourier transform (FFT) pattern shows that reflections at 6.87, 5.02, and 3.95 Å are associated with (111), (120), and (022), respectively. The angles between the (111) and (120) vectors and the (111) and (022) vectors are 38.2 and 83.2°, respectively, in good agreement with the angles of the ideal reciprocal lattice of the orthorhombic unit

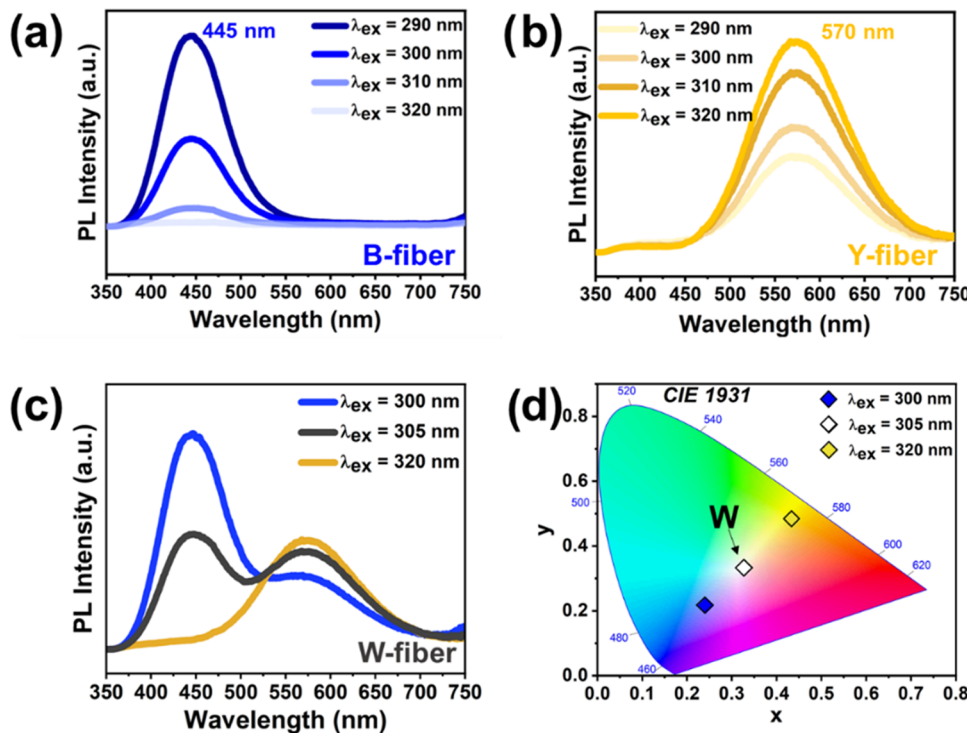


**Figure 3.** PL spectra of (a) B-fiber and (b) Y-fiber under different excitation wavelengths from 290 to 320 nm. (c) PL spectra and (d) CIE color coordinates of mixed two colors of B- and Y-fibers obtained by using dual-nozzle electrospinning under different excitation wavelengths from 300 to 320 nm.

cell. The reciprocal lattice constants of  $\text{Cs}_3\text{Cu}_2\text{I}_5$  perovskites are  $a^* = 0.0701 \text{ \AA}^{-1}$ ,  $b^* = 0.0989 \text{ \AA}^{-1}$ ,  $c^* = 0.0861 \text{ \AA}^{-1}$ ,  $\alpha^* = 90^\circ$ ,  $\beta^* = 90^\circ$ , and  $\gamma^* = 90^\circ$ .<sup>28</sup>

The cross-sectional TEM image of the Y-fiber sample also shows a microstructure similar to that of the B-fiber sample. Figure 4e presents the  $\text{CsCu}_2\text{I}_3$  perovskite nanocrystals in the polystyrene fiber, for which the crystallinity is comparable to  $\text{Cs}_3\text{Cu}_2\text{I}_5$  crystals. In Figure 4f, the FFT pattern indicates the (110) and (111) planes, and the angle between them is  $78.0^\circ$ , which matches well with the reciprocal lattice of  $\text{CsCu}_2\text{I}_3$  perovskites ( $a^* = 0.0952 \text{ \AA}^{-1}$ ,  $b^* = 0.0723 \text{ \AA}^{-1}$ ,  $c^* = 0.164 \text{ \AA}^{-1}$ ,  $\alpha^* = 90^\circ$ ,  $\beta^* = 90^\circ$ ,  $\gamma^* = 90^\circ$ ).<sup>29</sup> Although the  $\text{Cs}_3\text{Cu}_2\text{I}_5$  and  $\text{CsCu}_2\text{I}_3$  perovskite nanocrystals are rapidly crystallized in the polymer matrix, they have good crystal quality because of low formation energies and low growth temperature. The crystal phases of  $\text{Cs}_3\text{Cu}_2\text{I}_5$  and  $\text{CsCu}_2\text{I}_3$  perovskites could be controlled by the copper and cesium stoichiometry of the precursor solution. Additionally, the crystal structures of the B- and Y-fibers detached from the collector were studied using the XRD pattern to confirm the formation of perovskites within the PS polymer fibers (Figure 4g,h). The dominant diffraction peaks of the B-fiber are consistent with the standard orthorhombic  $\text{Cs}_3\text{Cu}_2\text{I}_5$  patterns, in which the diffraction peaks at  $24.15$ ,  $25.76$ ,  $26.46$ , and  $30.78^\circ$  correspond to the (122), (312), (222), and (004) planes, respectively.<sup>28</sup> In the Y-fiber, the peaks at  $10.70$ ,  $21.96$ ,  $26.12$ , and  $40.32^\circ$  correspond to the (110), (130), (221), and (042) planes of the orthorhombic phase ( $Cmcm$ ), respectively.<sup>29</sup> In both samples, the broad peaks at  $2\theta = 19.5^\circ$  result from amorphous organic polymer chains. No other peaks were detected above the detection limit, suggesting the high-phase purity of the perovskite phase and the absence of CsI and CuI salts in PS fibers.

IPNCs@PS fibers also show excellent water stability. The as-prepared B-fibers and  $\text{Cs}_3\text{Cu}_2\text{I}_5$  powder samples were immersed in deionized water to monitor water stability, where B-fibers maintained blue emission for 20 days under a 245 nm UV lamp, further confirming the strong stability in the presence of water. Unprotected  $\text{Cs}_3\text{Cu}_2\text{I}_5$  powders changed to  $\text{CsCu}_2\text{I}_3$  in only 1 min and decomposed to CuI in water in 5 min (Figure S3a). Generally, CsI is dissolved from  $\text{Cs}_3\text{Cu}_2\text{I}_5$  in the presence of moisture due to the high solubility of CsI in water, which leads to the formation of a yellow-emissive  $\text{CsCu}_2\text{I}_3$  product within several minutes.<sup>10,23</sup> However, the encapsulated  $\text{Cs}_3\text{Cu}_2\text{I}_5$  within PS fibers can effectively prevent the extraction of CsI and maintain long-term stability by protecting water efficiently.

Recently,  $\text{Cs}_3\text{Cu}_2\text{I}_5$  was encapsulated in PMMA as  $\text{Cs}_3\text{Cu}_2\text{I}_5@\text{PMMA}$ <sup>19,23</sup> and the silica matrix as  $\text{Cs}_3\text{Cu}_2\text{I}_5/\text{SiO}_2$ <sup>19,23</sup> to improve stability, which exhibited emission peaks at approximately 445 nm, like the present sample.  $\text{Cs}_3\text{Cu}_2\text{I}_5/\text{SiO}_2$  decomposes very fast under humid conditions into  $\text{CsCu}_2\text{I}_3$ ,<sup>19,23</sup> indicating that it is not appropriate in light-emitting device applications.  $\text{Cs}_3\text{Cu}_2\text{I}_5@\text{PMMA}$  composites fabricated by a complicated multistep process can tolerate 5 days in water.<sup>19,23</sup> Compared to these previous reports, the stability of present IPNCs@PS is remarkably improved, suggesting that the encapsulation of the IPNCs in the PS polymer matrix during the one-step electrospinning process is effective for enhancing resistance against the decomposition reaction of the IPNC samples. To confirm the crystal structure of IPNCs@PS fibers in water treatments, Figures S3b and S4 provide the XRD patterns of IPNCs@PS fibers, which exhibit no obvious change, representing excellent water stability. Figure S3b shows that the diffraction patterns for the (122) and (222) planes of the B-fiber were maintained in water

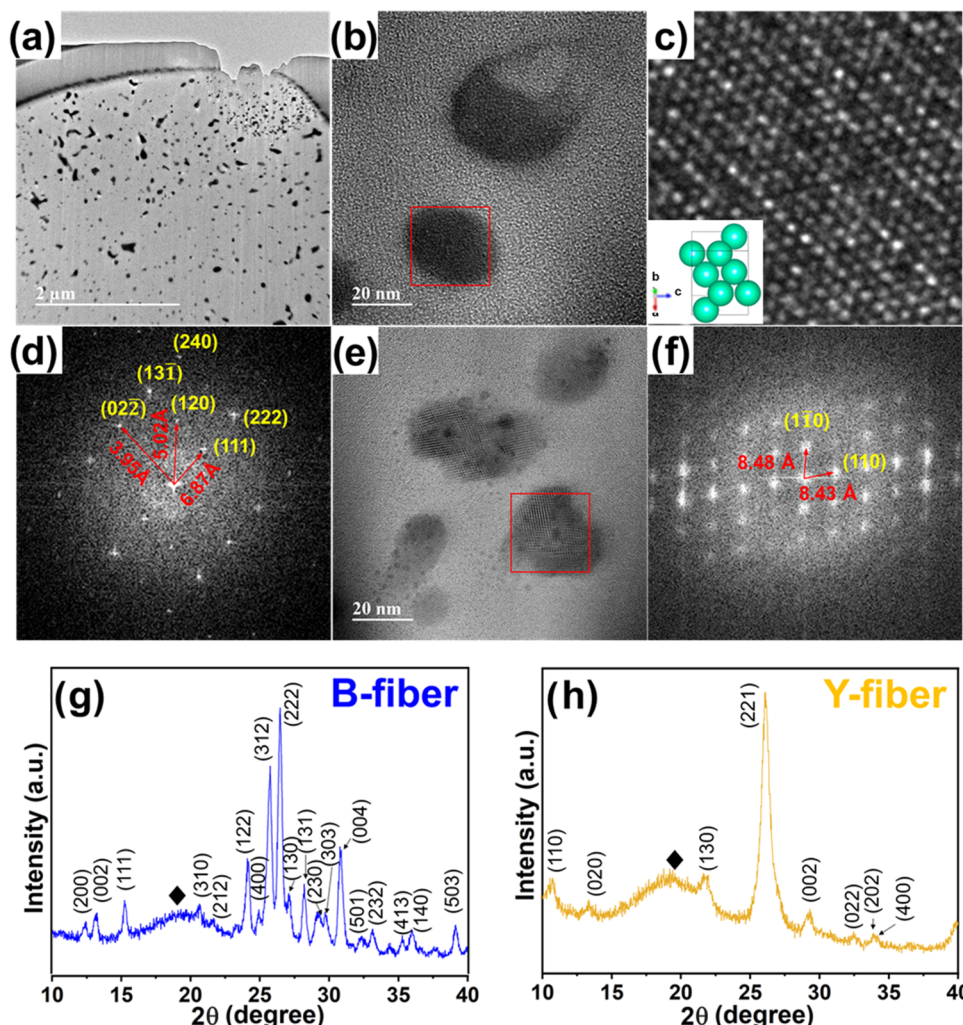


**Figure 4.** (a, b) Cross-sectional TEM image of B-fiber, (c) HR-TEM image, and (d) fast Fourier transform (FFT) pattern corresponding to the red box of (b). The inset of (c) is the atomic structure of cesium atoms of  $\text{Cs}_3\text{Cu}_2\text{I}_5$  perovskites. (e) TEM image of the Y-fiber and (f) FFT pattern corresponding to the red box of (e). XRD patterns of the as-synthesized (g) B-fiber and (h) Y-fiber detached from the Al foil collector. The peaks attributed to PS phases in (g, h) are indicated by the diamond (♦).

treatment even after 20 days. The diffraction patterns for (130) and (221) planes in the Y-fiber also remained, as shown in Figure S4. In both samples, the XRD peaks demonstrate perovskite polycrystalline samples and an aluminum hydroxide thin layer on aluminum metal substrates.

**3.3. Transparent and Flexible IPNCs@PS@PDMS Films.** We fabricated free-standing IPNCs@PS@PDMS films by coating PDMS on IPNCs@PS to improve physical strength, elasticity, and water stability compared to the as-prepared IPNCs@PS fibers<sup>31–33</sup> (Figure 5). The transmittance of IPNCs@PS nanofibers was quite low due to the light scattering of the exposed PS fiber. The light scattering can be strongly reduced by changing the PS surface environment of IPNCs@PS nanofibers through the infiltration of PDMS because the air in the pores between the nanofibers is replaced by PDMS.<sup>34</sup> The transmittance is influenced by factors such as the reflection index, which depends on the refractive index (RI) of the two materials forming the interface. This phenomenon can be described by the following formula<sup>35</sup>

$$r = [(n_s - n_f)/(n_s + n_f)]^2$$

Here,  $r$  is the reflective coefficient, and  $n_s$  and  $n_f$  are the RIs of the surrounding medium (air, PDMS) and the fibers, respectively. The RIs of air, PDMS, and PS nanofiber are 1.00, 1.55, and 1.51, respectively.<sup>35,36</sup> Thus, the light reflection at PS nanofiber/PDMS interfaces is much less than that at the PS nanofiber/air interfaces, demonstrating higher transmittance for IPNCs@PS@PDMS films than that for IPNCs@PS nanofibers. The transmittance of the PDMS substrate was approximately 95%, and even after the addition of the IPNCs@PS nanofiber into PDMS, the transmittance was still high, exceeding 80% in the visible wavelength range (Figure 5a). Although the transmittance of IPNCs@PS@PDMS was high due to the reduction of light scattering, it still showed strong PL emission, indicating that changes in light reflection related to the surrounding medium rarely affect PL emission.

The IPNCs@PS@PDMS film exhibited strong PL emission under a 245 nm UV lamp after 100% tensile strain (Figures 5b and S5). To analyze the optical properties of IPNCs@PS@PDMS under uniaxial tensile strain, the luminescence spectrum of the as-prepared films was explored under 300 and 320 nm excitation wavelengths. As shown in Figure 5c,d, the samples

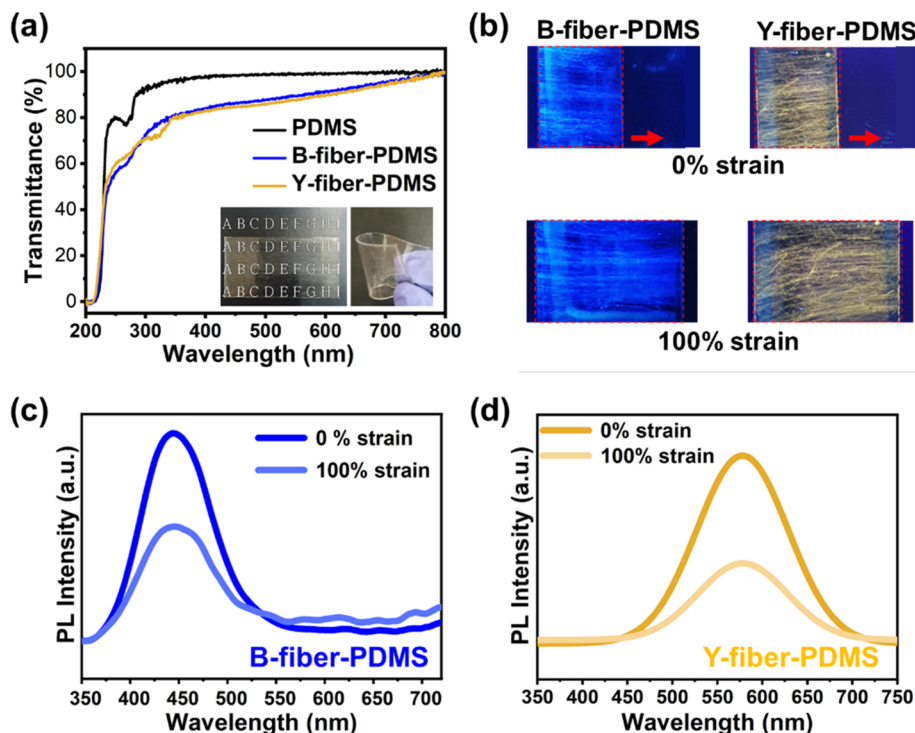


**Figure 5.** (a) UV-vis transmittance spectra of the B-fiber-PDMS, Y-fiber-PDMS, and PDMS. Transparent and flexible characterization is shown in the inset. Evolution of (b) photographic images, and PL spectra of the (c) B-fiber-PDMS and (d) Y-fiber-PDMS under uniaxial tensile strain.

exhibit emission peaks at 445 and 570 nm that are consistent with the known peak positions of  $\text{Cs}_3\text{Cu}_2\text{I}_5$  and  $\text{CsCu}_2\text{I}_3$ , respectively. The PL intensity decreased by approximately 50% at 100% tensile strain because the IPNC density per unit area decreased during stretching, which can be expressed using the following scaling law<sup>30</sup>

$$I/I_0 \propto \eta/\eta_0 \propto A_0/A$$

Here,  $I$  and  $I_0$  are luminescence intensities,  $\eta$  and  $\eta_0$  are the real number densities of phosphors, and  $A$  and  $A_0$  are the active areas in the stretched and unstretched states, respectively.

The area of IPNCs@PS@PDMS increased approximately 2-fold at 100% tensile strain compared to the samples without tensile strain. We expect (i) a decrease in  $\eta$  as  $A$  increases and (ii) a decrease in  $I$  as  $\eta$  per unit area decreases. The values of  $I/I_0$  in the luminescence spectrum at 100% tensile strain measured for the fixed area of IPNCs@PS@PDMS sized  $1 \times 1 \text{ cm}^2$  were 0.54 and 0.45 in Y-fiber-PDMS and B-fiber-PDMS, respectively, which are reasonably consistent with the theoretical data. IPNCs@PS@PDMS films are able to increase up to 300% tensile strain, and their PL intensity decreases by following the scaling law, as shown in Figure S6.

Although PDMS composites on electrospun nanofibers have been widely reported in creating flexible transparent matrices,<sup>36</sup> the optical properties of the perovskite-embedded nanofibers into PDMS have rarely been reported to the best of our knowledge. The present IPNCs@PS@PDMS films can be applied on a large-scale area by a simple two-step method without surfactants, showing strong blue and yellow PL emissions without a shift of the PL peak under tensile strain while demonstrating highly stretchable and physical strength characteristics. Notably, the IPNCs@PS@PDMS film exhibited strong PL emission even after 100% tensile strain and release were repeated up to 100 times (Figure S7). The

perovskites embedded in two matrices of PS and PDMS are strongly emissive Cs–Cu–I perovskites with good physicochemical properties such as high flexibility, transparency, and resistance to water. Considering the highly flexible and humidity-resistant characteristics, IPNCs@PS@PDMS films have great potential for use in wearable light-emitting devices.

## 4. CONCLUSIONS

In this study, we successfully fabricated  $\text{Cs}_3\text{Cu}_2\text{I}_5$  and  $\text{CsCu}_2\text{I}_3$  encapsulated within PS fibers using electrospinning. These fibers showed highly uniform and strong blue and yellow PL emissions with no significant defects with high reproducibility. The high-quality white emission film was obtained by mixing B- and Y-fibers in a facile manner using dual-nozzle electrospinning, resulting in a CIE coordinate of (0.31, 0.31), showing a white region with a CCT of 6635 K, which is a promising candidate in applications in lighting fields. The as-fabricated B- and Y-fibers exhibited remarkably improved water stabilities by isolating water efficiently due to the smooth, dense PS polymer matrix serving as a passivation layer. In addition, we applied a PDMS elastomer coating on IPNCs@PS. The fabricated materials are transparent, flexible, and stable in the ambient environment. They exhibit strong PL emission without peak shift at 100% tensile strain. IPNCs@PS@PDMS provides a facile and efficient application for cost-efficient and large-scale production, and PL emissions can be readily tuned, suggesting their promising applications in optoelectronic devices.

## ■ ASSOCIATED CONTENT

### ● Supporting Information

The Supporting Information is available free of charge at <https://pubs.acs.org/doi/10.1021/acsanm.2c04261>.

Photographs of the prepared films; XRD patterns of the samples before and after 20 days in water; PL spectra of samples before and after tensile strain; and ICP results of B- and Y-fibers ([PDF](#))

## AUTHOR INFORMATION

### Corresponding Authors

Min Wook Lee – Institute of Advanced Composite Materials, Korea Institute of Science and Technology (KIST), Wanju-gun 55324 Jeonbuk-do, Republic of Korea;  [orcid.org/0000-0003-3256-1067](#); Email: [mwlee0713@kist.re.kr](mailto:mwlee0713@kist.re.kr)

Ho Seong Jang – Materials Architecturing Research Center, Korea Institute of Science and Technology (KIST), Seoul 02792, Republic of Korea;  [orcid.org/0000-0002-2031-1303](#); Email: [msekorea@kist.re.kr](mailto:msekorea@kist.re.kr)

Duk-Young Jung – Department of Chemistry and Sungkyun Advanced Institute of NanoTechnology (SAINT), Sungkyunkwan University, Suwon 16419 Gyeonggi-do, Republic of Korea;  [orcid.org/0000-0003-3152-6382](#); Email: [dyjung@skku.edu](mailto:dyjung@skku.edu)

### Authors

Yongju Lee – Department of Chemistry and Sungkyun Advanced Institute of NanoTechnology (SAINT), Sungkyunkwan University, Suwon 16419 Gyeonggi-do, Republic of Korea

Ji-Hyun Cha – Department of Chemistry, Chungnam National University, Daejeon 34134, Republic of Korea

Heejin Kim – Institute of Advanced Composite Materials, Korea Institute of Science and Technology (KIST), Wanju-gun 55324 Jeonbuk-do, Republic of Korea

Ja Yeon Lee – Materials Architecturing Research Center, Korea Institute of Science and Technology (KIST), Seoul 02792, Republic of Korea

Complete contact information is available at:

<https://pubs.acs.org/10.1021/acsanm.2c04261>

### Author Contributions

Y.L., J.-H.C., and H.K. contributed equally to this work.

### Notes

The authors declare no competing financial interest.

## ACKNOWLEDGMENTS

This research was supported by the Basic Research Lab (2022R1A4A1019296), by Korea Initiative for fostering University of Research and Innovation Program (2020M3H1A1077095) and (2022R1A2C2005943) of the National Research Foundation (Ministry of Science and ICT of Korea). J.-H. Cha acknowledges Sejong Science Fellowship Grants (2021R1C1C2011591).

## REFERENCES

- (1) Swarnkar, A.; Marshall, A. R.; Sanehira, E. M.; Chernomordik, B. D.; Moore, D. T.; Christians, J. A.; Chakrabarti, T.; Luther, J. M. Quantum dot-induced phase stabilization of  $\alpha$ -CsPbI<sub>3</sub> perovskite for high-efficiency photovoltaics. *Science* **2016**, *354*, 92–95.
- (2) Li, G.; Rivarola, F. W. R.; Davis, N. J.; Bai, S.; Jellicoe, T. C.; de la Peña, F.; Hou, S.; Ducati, C.; Gao, F.; Friend, R. H.; et al. Highly efficient perovskite nanocrystal light-emitting diodes enabled by a universal crosslinking method. *Adv. Mater.* **2016**, *28*, 3528–3534.
- (3) Song, J.; Xu, L.; Li, J.; Xue, J.; Dong, Y.; Li, X.; Zeng, H. Monolayer and few-layer all-inorganic perovskites as a new family of

two-dimensional semiconductors for printable optoelectronic devices. *Adv. Mater.* **2016**, *28*, 4861–4869.

(4) Cha, J.-H.; Han, J. H.; Yin, W.; Park, C.; Park, Y.; Ahn, T. K.; Cho, J. H.; Jung, D.-Y. Photoresponse of CsPbBr<sub>3</sub> and Cs<sub>4</sub>PbBr<sub>6</sub> perovskite single crystals. *J. Phys. Chem. Lett.* **2017**, *8*, 565–570.

(5) Cha, J.-H.; Lee, H.-J.; Kim, S. H.; Ko, K. C.; Suh, B. J.; Han, O. H.; Jung, D.-Y. Superparamagnetism of green emissive Cs<sub>4</sub>PbBr<sub>6</sub> zero-dimensional perovskite crystals. *ACS Energy Lett.* **2020**, *5*, 2208–2216.

(6) Wang, A.; Guo, Y.; Muhammad, F.; Deng, Z. Controlled synthesis of lead-free cesium tin halide perovskite cubic nanocages with high stability. *Chem. Mater.* **2017**, *29*, 6493–6501.

(7) Benin, B. M.; Dirin, D. N.; Morad, V.; Wörle, M.; Yakunin, S.; Rainò, G.; Nazarenko, O.; Fischer, M.; Infante, I.; Kovalenko, M. V. Highly emissive self-trapped excitons in fully inorganic zero-dimensional tin halides. *Angew. Chem., Int. Ed.* **2018**, *57*, 11329–11333.

(8) Leng, M.; Yang, Y.; Zeng, K.; Chen, Z.; Tan, Z.; Li, S.; Li, J.; Xu, B.; Li, D.; Hautzinger, M. P.; et al. All-inorganic bismuth-based perovskite quantum dots with bright blue photoluminescence and excellent stability. *Adv. Funct. Mater.* **2018**, *28*, 1704446–1704456.

(9) Zhou, L.; Liao, J. F.; Huang, Z. G.; Wei, J. H.; Wang, X. D.; Li, W. G.; Chen, H. Y.; Kuang, D. B.; Su, C. Y. A highly red-emissive lead-free indium-based perovskite single crystal for sensitive water detection. *Angew. Chem.* **2019**, *131*, 5331–5335.

(10) Zhang, X.; Zhou, B.; Chen, X.; Yu, W. W. Reversible Transformation between Cs<sub>3</sub>Cu<sub>2</sub>I<sub>5</sub> and CsCu<sub>2</sub>I<sub>3</sub> Perovskite Derivatives and Its Anticounterfeiting Application. *Inorg. Chem.* **2022**, *61*, 399–405.

(11) Xie, L.; Chen, B.; Zhang, F.; Zhao, Z.; Wang, X.; Shi, L.; Liu, Y.; Huang, L.; Liu, R.; Zou, B.; Wang, Y. Highly luminescent and stable lead-free cesium copper halide perovskite powders for UV-pumped phosphor-converted light-emitting diodes. *Photonics Res.* **2020**, *8*, 768–775.

(12) Zhang, F.; Zhao, Z.; Chen, B.; Zheng, H.; Huang, L.; Liu, Y.; Wang, Y.; Rogach, A. L. Strongly emissive lead-free 0D Cs<sub>3</sub>Cu<sub>2</sub>I<sub>5</sub> perovskites synthesized by a room temperature solvent evaporation crystallization for down-conversion light-emitting devices and fluorescent inks. *Adv. Opt. Mater.* **2020**, *8*, No. 1901723.

(13) Grandhi, G. K.; Viswanath, N.; Cho, H. B.; Han, J. H.; Kim, S. M.; Choi, S.; Im, W. B. Mechanochemistry as a green route: Synthesis, thermal stability, and postsynthetic reversible phase transformation of highly-luminescent cesium copper halides. *J. Phys. Chem. Lett.* **2020**, *11*, 7723–7729.

(14) Cheng, P.; Sun, L.; Feng, L.; Yang, S.; Yang, Y.; Zheng, D.; Zhao, Y.; Sang, Y.; Zhang, R.; Wei, D.; et al. Colloidal synthesis and optical properties of all-inorganic low-dimensional cesium copper halide nanocrystals. *Angew. Chem.* **2019**, *131*, 16233–16237.

(15) Le, T.-H.; Lee, S.; Jo, H.; Kim, M.; Lee, J.; Chang, M.; Yoon, H. Deep Exciton Self-Trapping Cu-Based Perovskite Nanocrystals for Optoelectronic Applications. *ACS Appl. Nano Mater.* **2021**, *4*, 7621–7627.

(16) Yuan, D. Air-stable bulk halide single-crystal scintillator Cs<sub>3</sub>Cu<sub>2</sub>I<sub>5</sub> by melt growth: intrinsic and Tl doped with high light yield. *ACS Appl. Mater. Interfaces* **2020**, *12*, 38333–38340.

(17) Ma, J.; Xia, X.; Yan, S.; Li, Y.; Liang, W.; Yan, J.; Chen, X.; Wu, D.; Li, X.; Shi, Z. Stable and self-powered solar-blind ultraviolet photodetectors based on a Cs<sub>3</sub>Cu<sub>2</sub>I<sub>5</sub>/ $\beta$ -Ga<sub>2</sub>O<sub>3</sub> heterojunction prepared by dual-source vapor codeposition. *ACS Appl. Mater. Interfaces* **2021**, *13*, 15409–15419.

(18) Liu, X.; Yu, Y.; Yuan, F.; Zhao, C.; Dong, H.; Jiao, B.; Wu, Z. Vacuum dual-source thermal-deposited lead-free Cs<sub>3</sub>Cu<sub>2</sub>I<sub>5</sub> films with high photoluminescence quantum yield for deep-blue light-emitting diodes. *ACS Appl. Mater. Interfaces* **2020**, *12*, 52967–52975.

(19) Zhang, F.; Liang, W.; Wang, L.; Ma, Z.; Ji, X.; Wang, M.; Wang, Y.; Chen, X.; Wu, D.; Li, X.; et al. Moisture-induced reversible phase conversion of cesium copper iodine nanocrystals enables advanced anti-counterfeiting. *Adv. Funct. Mater.* **2021**, *31*, No. 2105771.

- (20) Jiang, T.; Wang, J.; Xie, L.; Bai, C.; Wang, M.; Wu, Y.; Zhang, F.; Zhao, Y.; Chen, B.; Wang, Y. In Situ Fabrication of Lead-Free  $\text{Cs}_3\text{Cu}_2\text{I}_5$  Nanostructures Embedded in Poly (Vinylidene Fluoride) Electrospun Fibers for Polarized Emission. *ACS Appl. Nano Mater.* **2022**, *5*, S08–S16.
- (21) Wang, L.-T.; Ma, Z.-Z.; Zhang, F.; Wang, M.; Chen, X.; Wu, D.; Tian, Y.-T.; Li, X.-J.; Shi, Z.-F. Stable down-conversion white light-emitting devices based on highly luminescent copper halides synthesized at room temperature. *J. Mater. Chem. C* **2021**, *9*, 6151–6159.
- (22) Liu, S.; Yue, Y.; Zhang, X.; Wang, C.; Yang, G.; Zhu, D. A controllable and reversible phase transformation between all-inorganic perovskites for white light emitting diodes. *J. Mater. Chem. C* **2020**, *8*, 8374–8379.
- (23) Wang, Y.; Yan, Y.; Li, D.; Zhao, W.; Chen, S.; Zhong, Q.; Liu, J.; Diarra, F.; Cao, M.; Zhang, Q. Reversible transformation of all-inorganic copper halide perovskite nanocrystals for anti-counterfeiting. *Dalton Trans.* **2021**, *50*, 12826–12830.
- (24) Ercan, E.; Tsai, P.-C.; Chen, J.-Y.; Lam, J.-Y.; Hsu, L.-C.; Chueh, C.-C.; Chen, W.-C. Stretchable and Ambient Stable Perovskite/Polymer Luminous Hybrid Nanofibers of Multicolor Fiber Mats and Their White LED Applications. *ACS Appl. Mater. Interfaces* **2019**, *11*, 23605–23615.
- (25) Hui, Y.; Chen, S.; Lin, R.; Zheng, W.; Huang, F. Photophysics in  $\text{Cs}_3\text{Cu}_2\text{I}_5$  and  $\text{CsCu}_2\text{I}_3$ . *Mater. Chem. Front.* **2021**, *5*, 7088–7107.
- (26) Cha, J.-H.; Kim, H.; Lee, Y.; Kim, S.-J.; Lee, M. W.; Kim, J.; Jung, D.-Y. Nanoscale optical imaging of perovskite nanocrystals directly embedded in polymer fiber. *Compos. Sci. Technol.* **2019**, *181*, 107666–107671.
- (27) Nývlt, J.; Šohnel, O.; Matuchova, M.; Broul, M. *The Kinetics of Industrial Crystallization*; Elsevier, 1985; p 19.
- (28) Bigalke, K. P.; Hans, A.; Hartl, H. Synthese und Strukturuntersuchungen von Iodocupraten (I). IX. Synthese und Kristallstrukturen von  $\text{Cs}_3\text{Cu}_2\text{I}_5$  und  $\text{RbCu}_2\text{I}_3$ . *Z. Anorg. Allg. Chem.* **1988**, *563*, 96–104.
- (29) Lin, R.; Guo, Q.; Zhu, Q.; Zhu, Y.; Zheng, W.; Huang, F. All-inorganic  $\text{CsCu}_2\text{I}_3$  single crystal with high-PLQY ( $\approx 15.7\%$ ) intrinsic white-light emission via strongly localized 1D excitonic recombination. *Adv. Mater.* **2019**, *31*, No. 1905079.
- (30) Zhou, H.; Park, J.; Lee, Y.; Park, J. M.; Kim, J. H.; Kim, J. S.; Lee, H. D.; Jo, S. H.; Cai, X.; Li, L.; et al. Water Passivation of Perovskite Nanocrystals Enables Air-Stable Intrinsically Stretchable Color-Conversion Layers for Stretchable Displays. *Adv. Mater.* **2020**, *32*, No. 2001989.
- (31) Gu, Z.; Huang, Z.; Hu, X.; Wang, Y.; Li, L.; Li, M.; Song, Y. In situ inkjet printing of the perovskite single-crystal array-embedded polydimethylsiloxane film for wearable light-emitting devices. *ACS Appl. Mater. Interfaces* **2020**, *12*, 22157–22162.
- (32) Gong, Y.; Shen, J.; Zhu, Y.; Yang, X.; Zhang, L.; Li, C. Stretch induced photoluminescence enhanced perovskite quantum dot polymer composites. *J. Mater. Chem. C* **2020**, *8*, 1413–1420.
- (33) Lee, M. W.; An, S.; Lee, C.; Liou, M.; Yarin, A. L.; Yoon, S. S. Self-healing transparent core–shell nanofiber coatings for anti-corrosive protection. *J. Mater. Chem. A* **2014**, *2*, 7045–7053.
- (34) Tang, C.; Liu, H. Cellulose nanofiber reinforced poly (vinyl alcohol) composite film with high visible light transmittance. *Composites, Part A* **2008**, *39*, 1638–1643.
- (35) Mark, J. E. *Physical Properties of Polymers Handbook*; Springer, 2007.
- (36) An, S.; Liou, M.; Song, K. Y.; Jo, H. S.; Lee, M. W.; Al-Deyab, S. S.; Yarin, A. L.; Yoon, S. S. Highly flexible transparent self-healing composite based on electrospun core–shell nanofibers produced by coaxial electrospinning for anti-corrosion and electrical insulation. *Nanoscale* **2015**, *7*, 17778–17785.

## □ Recommended by ACS

### Multicolor Display Fabricated via Stacking CW Laser-Patterned Perovskite Films

Lin Nie, Xuhui Xu, et al.

APRIL 03, 2023

ACS ENERGY LETTERS

READ ↗

### Zn<sub>2</sub>BS<sub>3</sub>Br: An Infrared Nonlinear Optical Material with Significant Dual-Property Enhancements Designed through a Template Grafting Strategy

Chun-Li Hu, Jiang-Gao Mao, et al.

MARCH 15, 2023

CHEMISTRY OF MATERIALS

READ ↗

### Highly Crystalline CsPbBr<sub>3</sub> Perovskite Nanoparticles for Liquid Crystal Displays

Wenqiang Ma, Lin Yang, et al.

FEBRUARY 28, 2023

ACS APPLIED NANO MATERIALS

READ ↗

### Polymer-Mediated *In Situ* Growth of Perovskite Nanocrystals in Electrospinning: Design of Composite Nanofiber-Based Highly Efficient Luminescent Solar Con...

Heeyoon Oh, Minwoo Park, et al.

NOVEMBER 23, 2022

ACS APPLIED ENERGY MATERIALS

READ ↗

Get More Suggestions >